Fuel Cells DOI: 10.1002/fuce.201300174

ORIGINAL RESEARCH PAPER

In Situ Measurements on Solid Oxide Fuel Cell Cathodes – Simultaneous X-Ray Absorption and AC Impedance Spectroscopy on Symmetrical Cells

R. J. Woolley[1], M. P. Ryan[1, 2], S. J. Skinner[1]*

[1] Department of Materials, Imperial College London, London SW7 2AZ, UK
[2] London Centre for Nanotechnology, Department of Materials, Imperial College London, London SW7 2AZ, UK

Received July 31, 2013; accepted October 22, 2013; published online November 08, 2013

Abstract

A solid oxide fuel cell *in operando* is a complex multiphasic entity under electrical polarization and operating at high temperatures. In this work, we reproduce these conditions while studying transition metal redox chemistry *in situ* at the cathode. This was achieved by building a furnace that allowed for X-ray absorption near-edge structure and AC impedance spectroscopy data to be obtained simultaneously on symmetrical cells while at operating temperatures. The cell electrodes consisted of phases from the Ruddlesden–Popper family; $La_2NiO_{4+\delta}$, $La_4Ni_3O_{10-\delta}$, and composites thereof. The redox chemistry of nickel in these cathodes was probed *in situ* through investigation of changes in the position of the X-ray absorption K-edge. An oxidation state reduction (Ni^{3+} to Ni^{2+}) was observed on heating the cells; this was correlated to changing concentrations of ionic charge carriers in the electrode. Polarizing the cells resulted in dramatic changes to their electrical performance but not to the bulk redox chemistry of the electrode. The implications of this with respect to explaining the polarization behavior are discussed.

Keywords: *In Situ* Characterization, La_2NiO_4, $La_4Ni_3O_{10}$, Nickel, Ruddlesden–Popper, SOFC Cathode, XANES, X-Ray Absorption Spectroscopy

1 Introduction

Solid oxide fuel cells (SOFCs) are electrochemical energy conversion devices with many attractive properties; however barriers to their commercialization still exist. One of the most significant is performance degradation during operation. Improved *in situ* characterization methods are required in order to understand the processes involved in this. Much progress has recently been made in this area and has been reviewed by Brett et al. [1]. Considering this, it becomes apparent that relatively little attention has been paid to *in situ* studies of SOFC cathodes. This is surprising given that polarization losses and long-term degradation are seen as a major bottleneck limiting the deployment of commercial devices [2].

A powerful technique that is routinely used in SOFC research is AC impedance spectroscopy (ACIS). This allows for the quantification of *electrical* properties of SOFC cathode materials *in situ*, however there are few methods by which *chemical* properties can be probed *in situ*. Cathodes typically contain transition metal ions that play a key role as oxygen reduction occurs *via* their redox chemistry. Further to this, the level of any oxygen non-stoichiometry is often related to the average oxidation state of the transition metal. Changes in this can change the non-stoichiometry parameter, δ, which governs the number of charge carriers available for mixed ionic-electronic conductivity. For further understanding of SOFC cathode materials, it is hence desirable to develop techniques to directly probe transition metal redox chemistry in response to the changing conditions in the cell.

Recently, we presented work on *in situ* X-ray absorption near-edge structure (XANES) data collected on the Ruddlesden–Popper (R–P) phases $La_2NiO_{4+\delta}$ (L2N1) and $La_4Ni_3O_{10-\delta}$

[*] *Corresponding author, s.skinner@imperial.ac.uk*

(L4N3) at room temperature and 650 °C [3]. These materials were chosen, as they are promising candidates for SOFC cathodes; they present attractive ionic and electronic conductivities [4–8]. We have shown that the performance of these can be improved by the formation of a L2N1:L4N3 composite, giving best-in-class results [9]. An advantage of these materials with respect to *in situ* chemical studies is that they contain just the single redox-active element, nickel, so analysis at a single absorption edge is representative of the electrochemical state of the material. This means that data collection and analyses are much simplified over materials with more than one such element where coupled redox changes may occur. In our proof-of-concept study, we demonstrated that nickel oxidation state changes in L2N1 and L4N3 are indeed responsible for charge compensation of oxygen non-stoichiometry, and correlated these data to previous modeling work [10]. A reduction in the Ni oxidation state was observed *in situ* on heating to 650 °C. This was discussed with respect to changes in δ, i.e., changing concentrations of oxygen interstitials in L2N1 and vacancies in L4N3. Itoh et al. [11] have carried out similar work on the cathode material $La_{1-x}Sr_xCo_{1-y}Fe_yO_{3-\delta}$ (LSCF), probing the Co and Fe oxidation state. Both of these studies, however were carried out on powders dispersed in boron nitride; an arrangement clearly bearing little resemblance to the cathode of an SOFC. Advancing this initial work, we present *in situ* XANES data obtained for test symmetrical cells with L2N1/L4N3 electrodes at operating temperature. Further to this, we were able to collect ACIS data and polarize the cells simultaneously with the XANES studies. This required the development of custom equipment to be used at synchrotron light sources. We adopted a setup similar to Hagen et al. [12], and shall discuss ours in detail. We believe that this is a significant improvement for *in situ* SOFC studies and paves the way for detailed analyses of redox processes occurring at the cathode.

2 Experimental Methods

2.1 Materials Studied

Symmetrical cells for testing were prepared as per our previous report [9], briefly; inks were made containing varying amounts of L2N1 (CerPoTech, synthesized by a spray pyrolysis technique) and L4N3 (synthesized by a sol–gel method).

Table 1 Electrode details and nomenclature for symmetrical cells tested.

Electrode ink composition	Sintering regime	Nomenclature
$La_2NiO_{4+\delta}$[(a)]	1,000 C × 4 h	L2N1
60 wt.% $La_2NiO_{4+\delta}$ + 40 wt.% $La_4Ni_3O_{10-\delta}$	1,000 C × 4 h	60:40
50 wt.% $La_2NiO_{4+\delta}$ + 50 wt.% $La_4Ni_3O_{10-\delta}$	1,000 C × 4 h	50:50
40 wt.% $La_2NiO_{4+\delta}$ + 60 wt.% $La_4Ni_3O_{10-\delta}$	1,000 C × 4 h	40:60
$La_4Ni_3O_{10-\delta}$[(b)]	1,200 C × 4 h	L4N3

[(a)]Subsequently found to contain a small L4N3 impurity.
[(b)]Undergoes slight decomposition toward lower-order R–P phases and NiO on sintering at 1,200 °C.

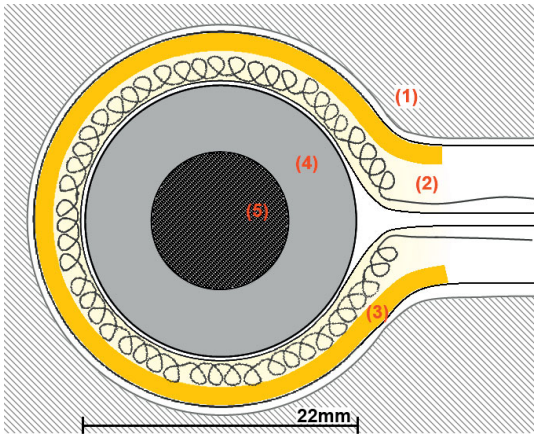

Fig. 1 Front view of sample holder held in alumina bricks. (1) insulating alumina brick; (2) IR element; (3) gold reflector in IR element; (4) Macor sample holder; (5) open part of sample holder, approx. 6 mm across, exposing coarse Pt mesh and electrode.

These were deposited onto dense $La_{0.8}Sr_{0.2}Ga_{0.8}Mg_{0.2}O_{3-\delta}$ (LSGM) electrolyte pellets and sintered as described in Table 1. It is to be noted that the L4N3 electrode required a high sintering temperature of 1,200 °C to give adequate adherence to the electrolyte. The finished cells were approx. ∅ 11 mm × 1.5 mm thick and were mounted in a furnace custom-designed to enable simultaneous *in situ* ACIS and XANES data collection.

2.2 Custom In Situ Furnace

Key requirements that were considered during the design of this equipment were the ability to heat a symmetrical solid oxide fuel cell to temperatures relevant to the "intermediate temperature" range (500–700 °C); to press a platinum mesh against the electrodes of the cell to provide electrical connections; and to position the cell in such a manner to allow for incident synchrotron light to impact upon one of the electrode layers. Heating was achieved using a circular infrared (IR) heating element (Omega 80008212 from Heraeus Noblelight). This has an in-built gold reflector that directs the IR radiation toward its center (Figure 1). IR heating is increasingly being used in such *in situ* rigs due to its compact nature and efficient heating [13]. Temperature was controlled by a Eurotherm 2116 controller. The internal diameter of the element was approx. 22 mm; a Macor sample holder was machined to fit inside this (Figure 2). It consists of male and female sections designed such that the symmetrical cell and platinum meshes fit inside. The two parts screw together holding the meshes firmly against each side of the symmetrical cell, providing the electrical connections. Each end of the holder is open allowing for a thermocouple to be positioned close to one of the electrodes and X-rays to be incident on the other. The X-rays first had to penetrate the Pt mesh so this was chosen to be relatively coarse, with an open area of 62.7% (Advent Research Materials Pt5425). Pt wires were spot-welded to the meshes, run out the open ends of the holder,

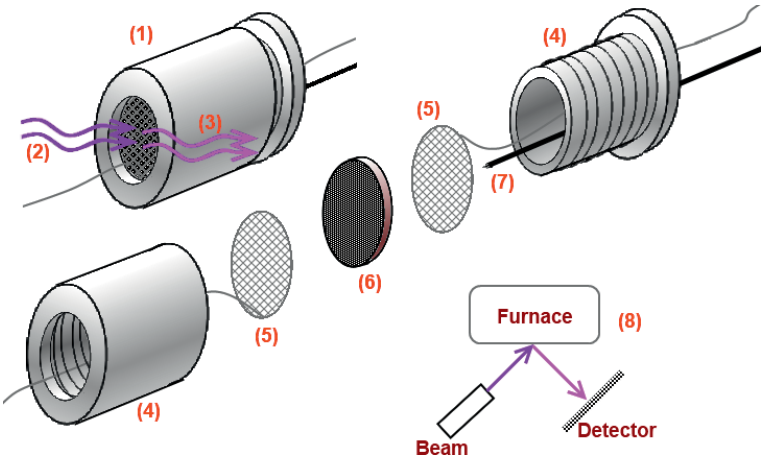

Fig. 2 Schematic diagram of sample holder. (1) Combined holder; (2) X-rays incident on exposed electrode; (3) fluorescent X-rays; (4) Open parts of machined Macor® holder – screw thread visible; (5) Pt meshes and electrical connections; (6) symmetrical cell; (7) K-type thermocouple; (8) plan view of furnace in beam hutch demonstrating fluorescence geometry.

and connected to a Voltalab 80 PGZ 402 Universal Potentiostat such that the cells were tested in a two-electrode manner.

The sample holder was positioned inside the IR heating element, holding the symmetrical cell in the center of the heated zone. The whole arrangement was supported in a cavity cut into insulating alumina bricks such that it was surrounded on five sides (Figure 1). On the final exposed face, alumina plates were used to create an aperture such that the X-rays were not blocked but radiative heat-loss from this face was minimized. The overall design was compact at approx. 150 mm × 80 mm × 80 mm; this small size combined with the focussed IR element allowed for fast heating and cooling. Temperatures around 600–700 °C were readily reached in less than 1 h and upon switching off the element the furnace cooled to room temperature on a similar timescale. To calibrate the temperature of symmetrical cells inside our custom *in situ* furnace, we compared area-specific resistance (ASR) values obtained for cells measured within the apparatus with those determined in our previous work using a standard ACIS set-up (Solartron 1260a FRA; 10^{6}–10^{-2} Hz; applied amplitude: 25 mV; 500–700 °C; under static laboratory atmosphere). An identical cell should display the same polarization resistance when at the same temperature in different furnaces. One of the composite 50:50 L2N1 + L4N3 cells remaining from our recent publication [9] was chosen for testing in this current study. By correlating the two data sets, we were able to correct the temperature read by the thermocouple of the custom furnace to the temperature of the symmetrical cell in its center; a difference of approximately 30° was found to be constant over the tested temperature range.

2.3 Further Experimental Details

Standard samples of L2N1 and L4N3 powders were used to verify the Ni edge positions ensuring electrode layers and dispersed powders gave similar results; these were prepared by mixing with hexagonal boron nitride (h-BN) and pressing into lozenges, which were mounted in the furnace used in our previous study [3]. All data were collected in static laboratory atmosphere.

XANES data were collected at beamline X10C at the National Synchrotron Light Source, Brookhaven National Laboratory, USA. Nickel is the only redox-active element in L2N1 and L4N3 so this study focussed on the Ni K-edge; 8,200–8,800 eV (the Ni metal K-edge is at 8333.0 eV). All data were obtained in fluorescence geometry – this is a necessity given the opaque nature of the cells tested. Background subtraction and normalization were achieved using the Athena GUI [14] for IFEFFIT [15] software. K-edge positions were deemed to be at a maximum in the first-derivative data; the precise position of this was found as a zero-crossing in the second derivative. A three-point smoothing algorithm was applied to ensure consistency in the identification of this position. ACIS data were collected from 10^{4} to 10^{-2} Hz with an AC amplitude of 25 mV. The effect of polarization was tested from 0 to ±2,400 mV. To facilitate comparison, XANES and ACIS data collection times were designed to be the same; approximately 20 min per measurement.

The penetration depth of the X-rays must be taken into account as this will be the region of the sample being probed by the technique. The attenuation length is defined as the depth into the material where the intensity of the X-rays has decreased to $1/e$ (≈37%) of the value at the surface. The Beer–Lambert law can be written as;

$$I = I_0 \exp(-\mu\rho x)$$

where I is the intensity at depth x, I_0 the intensity at the surface, μ the mass absorption coefficient, and ρ the material density. From this the attenuation depth is derived as;

$$x = \frac{1}{\mu\rho}$$

Using data from Henke et al. [16] and estimating that the porous electrode layer is 50% theoretical density the attenuation depth is calculated to be of the order of 10 µm. The thickness of the electrodes is approx. 30 µm [9]; the penetration depth is significant and the data therefore relevant to the bulk of the electrode. Information that is more surface-sensitive could be obtained using the same furnace setup by varying the X-ray incident angle, analogous to the "ReflEXAFS" technique [17, 18].

XRD data to confirm phase formation were collected on using a PANalytical X'Pert Pro MPD using Ni filtered Cu Kα radiation with tube voltage/current at 40 kV/40 mA.

3 Results

3.1 Room Temperature XANES

The room temperature nickel K-edge positions for the various symmetrical cell electrodes tested are presented in Table 2 and Figure 3 along with data for L2N1 and L4N3 powders diluted in h-BN. As a general trend, the K-edge position shifts toward higher energy as the amount of L4N3 is increased. This indicates a higher average nickel oxidation state in the electrode. It is apparent that the energy of the Ni K-edge in the L4N3 electrode is 0.7 eV lower than that of the L4N3 powder. This was anticipated from our experience in working with these phases and is explained *via* Figure 4. Here XRD patterns collected for the electrodes after testing are compared to as-received powders. For L4N3 extra peaks are present in the diffraction pattern from the electrode verses the powder material. These correspond to nickel oxide and the lower-order R–P phases L2N1 and L3N2 ($La_3Ni_2O_{7-\delta}$). These are present due to the slight decomposition that occurs in L4N3 at the sintering temperature of 1,200 °C. This will result in a higher Ni^{2+} content in the sintered electrode than in the pure powder sample and explains the lower K-edge position. These phase changes are fully evaluated in our previous work [9] by comparison to the relevant thermodynamic literature on the La–Ni–O system [19]. The edge position for the L2N1 electrode was found to be 0.2 eV higher than the L2N1 powder. This was not anticipated from our previous study but again can be explained by analysis of the XRD patterns in Figure 4. After testing, it was discovered that this electrode had been contaminated with a small amount of L4N3. This will increase the Ni^{3+} content compared to pure L2N1 hence shifting the Ni K-edge position of the electrode to higher energy. This example serves to illustrate the ability of XANES to identify small and potentially unexpected chemical changes occurring in SOFC materials.

3.2 High Temperature XANES

The K-edge positions at elevated temperatures are summarized in Table 2 and Figure 3. The different electrodes behave similarly; typically from room temperature to 620 °C the edge shifts toward lower energy by 0.2–0.3 eV implying a reduction in the nickel oxidation state. Some cells showed a further slight reduction between 620 and 670 °C. The exception was the L2N1 cell, which showed no reduction at 620 °C, but by 670 °C a reduction of a similar magnitude to the other cells. This could reflect the magnitude of the energy shifts observed, compared to the error estimated in the measurements at ±0.1 eV. Figure 5 shows XANES data for the 60:40 cell with the shift at high temperature evident. The sharp "glitch" indicated in the figure is an artifact from the X-ray spectrometer monochromator crystal. It was consistently at the same energy, which indicates that the monochromator calibration is stable; similar behavior has been reported previously on this beamline [20]. A pre-edge feature is visible at about 8,334 eV; this is due to a "forbidden" 1s → 3d transition. Distortions in the NiO_6 octahedra allow for p–d orbital mixing and relax selection rules. Over the course of the electrical testing to be described below the cells were at elevated temperature for up to 4 h with no change observed in the K-edge position over this period. Upon cooling to room temperature the K-edge positions returned to their pre-testing positions implying that the reduction at high temperatures is fully reversible. The behavior of the electrodes is consistent with the knowledge gained from our previous XANES studies on L2N1 and L4N3 powders [3] and corresponds to a reduction in the average oxidation state of approximately 0.1 for each phase between room and high temperature. For L2N1, this indicates that there will be fewer interstitial oxygen ions available for ionic conductivity (decreased δ in $La_2NiO_{4+\delta}$) whereas for L4N3 there will be a greater number of oxygen vacancies available (increased δ in $La_4Ni_3O_{10-\delta}$). The performance of the composite electrodes will be affected by a subtle interplay between these factors. That no shift in the K-edge is observed over the testing period suggests that the material is stable; this is important as durability is of paramount importance for SOFC materials. "Cyclability" is also a desired property possessed by these materials. This is demonstrated by the fact that the redox behavior is reversible, i.e., the K-edges return to their pre-testing values on cooling.

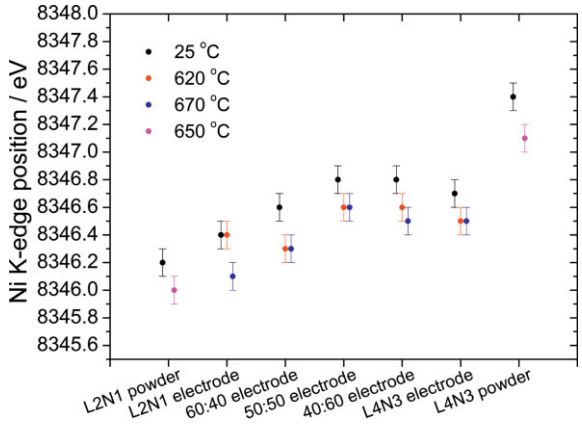

Fig. 3 Ni K-edge positions for powders and symmetrical cell electrodes at room and high temperatures.

Table 2 Ni K-edge positions at different temperatures for materials tested.

Sample	Nickel K-edge position[(a)]/eV			
	RT	620 °C	670 °C	650 °C
L2N1 powder	8346.2	–	–	8346.0
L4N3 powder	8347.4	–	–	8347.1
L2N1 cell	8346.4	8346.4	8346.1	–
60:40 cell	8346.6	8346.3	8346.3	–
50:50 cell	8346.8	8346.6	8346.6	–
40:60 cell	8346.8	8346.6	8346.5	–
L4N3 cell	8346.7	8346.5	8346.5	–

[(a)]Error in K-edge positions estimated at ±0.1 eV.

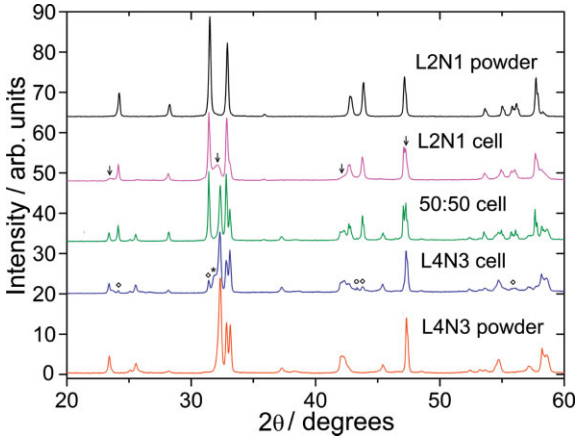

Fig. 4 XRD patterns of as-received L2N1 and L4N3 powders in comparison to symmetrical cell electrodes after testing. The L2N1 cell was found to contain a small L4N3 contamination (marked by arrows); the L4N3 cell has undergone slight decomposition toward NiO (circles), L2N1 (diamonds), and L3N2 (asterisks).

3.3 ACIS Data Under Open Circuit Voltage

Figure 6 shows typical ACIS data at 620 and 670 °C presented on a Nyquist plot; these were obtained from a 60:40 composite cell under open-circuit conditions and are representative for the rest of the electrodes. The background electrical noise evident in these data is due to the non-ideal environment at the synchrotron. The beamline setup required the electrical connections between the FRA and symmetrical cell to pass across a variety of other electrical equipment; some interference may result from this. Nevertheless, data are readily obtained and the electrode signal is strong. Table 3 gives the ASRs for the electrodes, which were estimated from the difference in the high and low frequency intercepts with $Z'' = 0$. The relative performances of the different electrodes

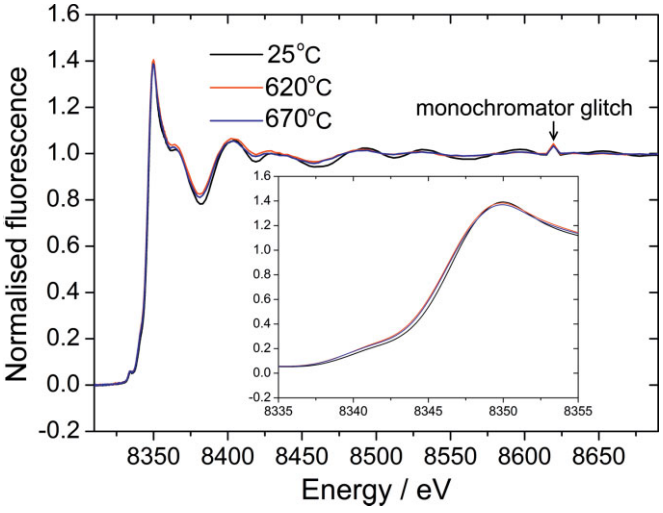

Fig. 5 Nickel K-edge XANES data at room temperature, 620, and 670 °C for 60:40 cell. Data are representative of all electrodes tested. Inset shows the region of the edge-jump with the shift toward lower energy at high temperature clearly evident. Glitch marked is due to an imperfection in the monochromator.

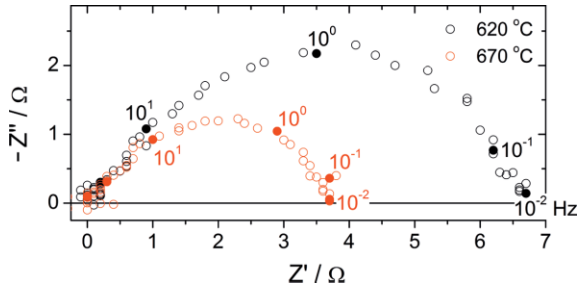

Fig. 6 ACIS data for 60:40 cell at 620 and 670 °C. Data normalized to zero inductance and series resistance.

tested in the *in situ* setup were consistent with our previous detailed study [9] with a 50:50 wt.% L2N1 + L4N3 composite electrode giving the best performance. It is to be noted that the act of collecting ACIS data under open-circuit had no observable effect on the XANES data.

3.4 ACIS and XANES Data Under Polarization

SOFCs are electrochemical devices and hence operate under polarization. This is typically of the order of 1 V so, to further simulate the conditions of an SOFC *in operando*, similar polarizations were applied to the symmetrical cells during data collection. This caused a pronounced change in the ACIS data. Arcs for all the cells contracted and became more depressed, the largest effect being for L4N3 as shown in Figure 7, indicating reduced cell resistance. The level of noise in the data increased markedly. This was particularly apparent at low frequencies where reliable data became hard to acquire.

XANES data collected during polarization showed *no change* from the open-circuit data for any of the cells. This was confirmed for the L2N1 cell for applied voltages to ±2.4 V. It was thought plausible that perhaps the nickel reduction that occurs during heating suppresses the possibility of any further redox changes due to an applied bias. ±2.4 V was applied to L2N1 at room temperature to test this, but again no change was seen in the K-edge position. Figure 8 displays the first derivative of the absorbance for these L2N1 XANES data. It is clear that the maximum in this, i.e., the Ni K-edge position, is invariant with polarization. These data lead to the conclusion that the bulk redox chemistry of nickel in these materials is dominated by thermal effects. Similar behavior has been observed for iron and cobalt redox chemistry in LSCF cathodes under smaller polarizations [12].

Table 3 Area specific resistances for symmetrical cells under open circuit voltage.

Electrode	ASR/Ω cm^2	
	620 °C	670 °C
L2N1	5.0	2.7
60:40	3.0	1.7
50:50	2.6	1.0
40:60	5.4	2.5
L4N3	15.0	6.3

4 Discussion

It must be noted that in this study we were *not* looking to explore in detail the effect of polarization on the *electrical* properties of these materials. The goal was to demonstrate that polarization does affect the performance, and to explore *in situ* any changes in *redox chemistry* linked to this. A detailed electrical study into polarization effects on La–Ni R–P phases has already been carried out by Pérez-Coll et al. [21]. They observed that DC polarization during ACIS testing leads to improved performances for L2N1 and L3N2 electrodes at high current fluxes, our work being consistent with this. L3N2 corresponds to the phase $La_3Ni_2O_{7-\delta}$, which has similar defect chemistry to the L4N3 studied here [22]. Pérez-Coll et al. however do not put forward a mechanism to explain their findings.

The effect of polarization on more-traditional perovskite SOFC cathode materials has received significant attention in the literature. Performance changes have been noted and various mechanisms have been proposed to explain these. These involve:

(a) partial reduction of the transition metal cation, leading to an increased number of oxygen vacancies, hence facilitating oxygen incorporation [23, 24],

(b) microstructural changes in the electrode that may lead to improved oxygen diffusion [25, 26],

(c) cation diffusion leading to enhanced electrode properties at the surface [27–30].

Considering the R–P phases explored in this work, analogous mechanisms could take place. For L4N3, a phase containing a significant concentration of oxygen vacancies [7], mechanism (a) above would correspond to

$$2Ni^{\bullet}_{Ni,R-P} + O^{x}_{O,R-P} + V^{\bullet\bullet}_{O,LSGM} + 2e \rightarrow 2Ni^{x}_{Ni,R-P} + O^{x}_{O,LSGM} + V^{\bullet\bullet}_{O,R-P}$$

where $Ni^{\bullet}_{Ni,R-P}$, $Ni^{x}_{Ni,R-P}$, $O^{x}_{O,R-P}$, and $V^{\bullet\bullet}_{O,R-P}$, respectively represent Ni^{3+}, Ni^{2+}, O^{2-}, and oxygen vacancies present in the R–P phase, and $V^{\bullet\bullet}_{O,LSGM}$ and $O^{x}_{O,LSGM}$ represent oxygen vacancies and O^{2-} in LSGM.

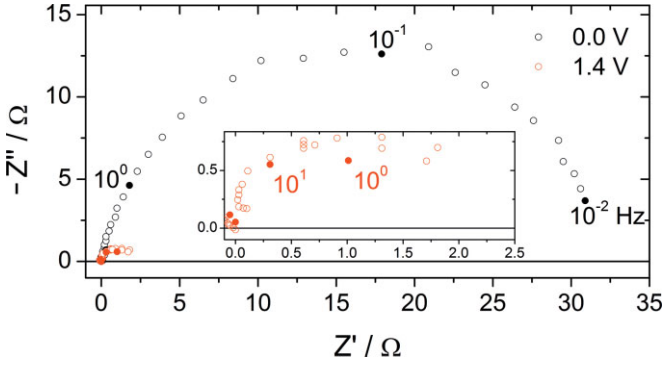

Fig. 7 ACIS data at 620 °C under open circuit and 1.4 V polarizations on L4N3 cell. Data normalized to zero inductance and series resistance. Inset: close-up of data at 1.4 V; points at frequencies below 10^0 Hz omitted for polarized cell.

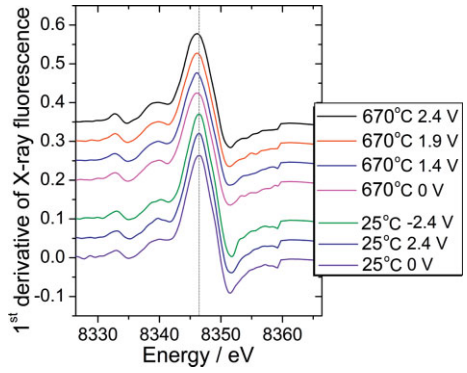

Fig. 8 First derivative of normalized fluorescence for L2N1 cell at room temperature and 670 °C, under different polarizations. Dashed line is at 8,346.4 eV, the K-edge position at room temperature. It is evident that the maximum of the first derivative is invariant with polarization.

This mechanism would lead to improved performance in L4N3 – this phase has a large number of Ni^{3+} ions available to be reduced and the creation of more oxygen vacancies should improve its cathode properties. However for L2N1 this is not the case. This phase has oxygen interstitials rather than vacancies [31] so cathodic polarization would reduce the concentration of these and impair the performance thus

$$2Ni^{\bullet}_{Ni,R-P} + O_{i,R-P} + V^{\bullet\bullet}_{O,LSGM} + 2e \rightarrow 2Ni^{x}_{Ni,R-P} + O^{x}_{O,LSGM}$$

where $O_{i,R-P}$ represents an interstitial O^{2-} in the R–P phase.

Mechanism (b) is considered unlikely as it is implausible that small microstructural changes in the electrode should be able to cause such significant changes to the ASR. When considering mechanism (c) the surface chemistry of the materials is an important factor. Low-energy ion scattering (LEIS) has revealed that L2N1 is terminated by a LaO layer [32]. Similar studies have yet to be carried out for the higher-order phases. Skinner and Kilner [5] and Smith and Norby [33] have shown that the activation energy for oxygen surface exchange in L2N1 is significantly greater than for diffusion. Opposite results have been found for perovskite materials [34] containing oxygen vacancies. It has been proposed by Li et al. [35] that the surface layer of LaO is the reason for the high activation energy seen for L2N1. Building on this with respect to mechanism (c), it is plausible that polarization-induced cation diffusion brings some nickel to the surface of the La–Ni R–P phases, leading to improved oxygen reduction catalysis. However, such a mechanism would be expected to lead to some persistence in the performance changes upon removal of the polarization; ions would take time relax back to their equilibrium position [27, 29]. Pérez-Coll observed no such persistence, seeming to eliminate mechanism (c).

This leads to a somewhat contradictory state. On the one hand, various aspects of mechanism (a) make it seem the most likely explanation, yet on the other hand we observed no changes in the nickel K-edge position throughout our testing. This could be explained if any nickel redox activity is confined to a surface region of the material, rather than

throughout the bulk. These may be beyond the sensitivity of the XANES measurements made in the current geometry. Alternatively, the redox behavior could be confined to a small region near the electrode/electrolyte interface. This region was not being probed in this study due to the penetration depth, and further experiments with thin electrodes could be carried out to rectify this. However, it is to be noted that Hagen et al. tested thin LSCF electrodes in a similar manner to this study. Their electrodes were fully-penetrated by the X-ray beam yet they did not see any effects of polarization on either the iron or cobalt absorption edges [12]. It is apparent that a complete explanation for the behavior of these La–Ni R–P phases under polarization has yet to be reached. What this study proves is that the bulk nickel redox chemistry in these materials is dominated by thermal effects. Therefore any proposed contribution of nickel redox to the electrochemical performance of these cathodes under polarization must occur at either the surface, or the electrolyte/electrode interface.

5 Conclusion

Novel equipment has been developed to enable simultaneous XANES and ACIS data to be collected *in situ* on symmetrical cells at temperatures relevant to IT-SOFCs. The combination of these powerful techniques is a great step toward further understanding of the processes occurring at SOFC cathodes *in operando*. This equipment was used to study electrodes consisting of L2N1, L4N3, and composites between the two. These were chosen as they are promising cathode materials, with the advantage of only having one multi-valent element – nickel – facilitating XANES testing and analyses.

The nickel K-edge was probed, with shifts toward lower or higher energy indicating different oxidation states being present in the bulk electrode material. On heating to 670 °C, i.e., to temperatures appropriate for IT-SOFC materials, the K-edge position moves to lower energy by 0.2–0.3 eV. This agrees with our XANES study on bulk powders [3] and correlates to a reduction in oxidation state of approximately 0.1. For L2N1, this will mean a decreased concentration of oxygen interstitials and for L4N3 an increased number of oxygen vacancies. Under OCV the ACIS data were as expected from our previous work [9], however when polarizing the cell significant changes were evident. Detailed studies of the electrical behavior of these materials have already been carried out [21], so we focussed on the chemical behavior. No changes were observed in the nickel K-edge position under polarizations of ±2.4 V, leading to the conclusion that the bulk nickel redox chemistry in these phases is dominated by thermal effects. Various mechanisms were considered, however a satisfactory explanation for the polarization effects is yet to be reached. If a mechanism does involve nickel redox behavior, this study shows that this must not be occurring over throughout the bulk of the electrode. Further, experiments should be carried out to deconvolute bulk and surface contributions; these could involve varying the thickness of the tested electrodes, as well as varying the incident angle of the X-rays. The equipment and techniques utilized during this work are considered to be an important step toward complete understanding of the processes occurring at the cathode of an SOFC.

Acknowledgments

Firstly the authors wish to express their fullest thanks to Dr. Ivelin Valkov for his invaluable contribution toward the development of the *in situ* furnace. We also acknowledge the Centre for Advanced Structural Ceramics at Imperial College London, and the EPSRC Supergen Fuel Cells program, for funding. Use of the National Synchrotron Light Source, Brookhaven National Laboratory, was supported by the U.S. Department of Energy, Office of Science, Office of Basic Energy Sciences, under Contract no. DE-AC02-98CH10886 and we thank Larry Fareria for his assistance at beamline X10C.

References

[1] D. J. L. Brett, A. R. Kucernak, P. Aguiar, S. C. Atkins, N. P. Brandon, R. Clague, L. F. Cohen, G. Hinds, C. Kalyvas, G. J. Offer, B. Ladewig, R. Maher, A. Marquis, P. Shearing, N. Vasileiadis, V. Vesovic, *Chemphyschem* **2010**, *11*, 2714.

[2] C. Sun, R. Hui, J. Roller, *J. Solid State Electrochem.* **2010**, *14*, 1125.

[3] R. J. Woolley, B. N. Illy, M. P. Ryan, S. J. Skinner, *J. Mater. Chem.* **2011**, *21*, 18592.

[4] V. V. Kharton, A. P. Viskup, E. N. Naumovich, F. M. B. Marques, *J. Mater. Chem.* **1999**, *9*, 2623.

[5] S. J. Skinner, J. A. Kilner, *Solid State Ionics* **2000**, *135*, 709.

[6] G. Amow, S. J. Skinner, *J. Solid State Electrochem.* **2006**, *10*, 538.

[7] G. Amow, I. Davidson, S. Skinner, *Solid State Ionics* **2006**, *177*, 1205.

[8] S. Takahashi, S. Nishimoto, M. Matsuda, M. Miyake, *J. Am. Ceram. Soc.* **2010**, *93*, 2329.

[9] R. J. Woolley, S. J. Skinner, *J. Power Sources* **2013**, *243*, 790.

[10] L. Minervini, R. W. Grimes, J. A. Kilner, K. E. Sickafus, *J. Mater. Chem.* **2000**, *10*, 2349.

[11] T. Itoh, S. Shirasaki, H. Ofuchi, S. Hirayama, T. Honma, M. Mori, M. Nakayama, *J. Fuel Cell Sci. Technol.* **2012**, *9*, 031004.

[12] A. Hagen, M. L. Traulsen, W.-R. Kiebach, B. S. Johansen, *J. Synchrotron. Rad.* **2012**, *19*, 400.

[13] S. J. Moorhouse, N. Vranjes, A. Jupe, M. Drakopoulos, D. O'Hare, *Rev. Sci. Instrum.* **2012**, *83*.

[14] B. Ravel, M. Newville, *J. Synchrotron. Rad.* **2005**, *12*, 537.

[15] M. Newville, *J. Synchrotron. Rad.* **2001**, *8*, 322.

[16] B. L. Henke, E. M. Gullikson, J. C. Davis, *At. Data Nucl. Data Tables* **1993**, *54*, 181.
[17] G. Martens, P. Rabe, *J. Phys. C: Solid State Phys.* **1981**, *14*, 1523.
[18] V. Lopez-Flores, S. Ansell, D. T. Bowron, S. Diaz-Moreno, S. Ramos, A. Munoz-Paez, *Rev. Sci. Instrum.* **2007**, *78*.
[19] M. Zinkevich, F. Aldinger, *J. Alloys Compd.* **2004**, *375*, 147.
[20] A. J. Davenport, M. Sansone, *J. Electrochem. Soc.* **1995**, *142*, 725.
[21] D. Pérez-Coll, A. Aguadero, M. J. Escudero, L. Daza, *J. Power Sources* **2009**, *192*, 2.
[22] Y. Kobayashi, S. Taniguchi, M. Kasai, M. Sato, T. Nishioka, M. Kontani, *J. Phys. Soc. Jpn.* **1996**, *65*, 3978.
[23] Y. Jiang, S. Wang, Y. Zhang, J. Yan, W. Li, *J. Electrochem. Soc.* **1998**, *145*, 373.
[24] H. Y. Lee, W. S. Cho, S. M. Oh, H. D. Wiemhofer, W. Gopel, *J. Electrochem. Soc.* **1995**, *142*, 2659.
[25] M. Kuznecov, P. Otschik, P. Obenaus, K. Eichler, W. Schaffrath, *Solid State Ionics* **2003**, *157*, 371.
[26] M. J. Jørgensen, P. Holtappels, C. C. Appel, *J.Appl. Electrochem.* **2000**, *30*, 411.
[27] W. Wang, S. P. Jiang, *Solid State Ionics* **2006**, *177*, 1361.
[28] A.-K. Huber, M. Falk, M. Rohnke, B. Luerssen, L. Gregoratti, M. Amati, J. Janek, *Phys. Chem. Chem. Phys.* **2012**, *14*, 751.
[29] F. S. Baumann, J. Fleig, M. Konuma, U. Starke, H.-U. Habermeier, J. Maier, *J. Electrochem. Soc.* **2005**, *152*, A2074.
[30] M. Finsterbusch, A. Lussier, J. A. Schaefer, Y. U. Idzerda, *Solid State Ionics* **2012**, *212*, 77.
[31] W. Paulus, A. Cousson, G. Dhalenne, J. Berthon, A. Revcolevschi, S. Hosoya, W. Treutmann, G. Heger, R. Le Toquin, *Solid State Sci.* **2002**, *4*, 565.
[32] M. Burriel, S. Wilkins, J. Hill, M. P. Ryan, S. J. Skinner, J. A. Kilner, in *9th European SOFC Forum* (Ed. P. Connor), Lucerne, Switzerland, **2010**, p. 10_43.
[33] J. B. Smith, T. Norby, *J. Electrochem. Soc.* **2006**, *153*, A233.
[34] R. A. De Souza, J. A. Kilner, *Solid State Ionics* **1999**, *126*, 153.
[35] Z. Li, T. Norby, R. Haugsrud, *J. Am. Ceram. Soc.* **2012**, *95*, 2065.

